Fermi National Accelerator Laboratory

FERMILAB-Pub-92/364

R&D on Mechanical Construction and Cooling of a 3-D Silicon Vertex Detector

Paul Lebrun, Carl Lindenmeyer, Linda Stutte, Herman Cease and Dan Chissus

Fermi National Accelerator Laboratory
P.O. Box 500, Batavia, Illinois 60510

December 1992

Submitted to *Nuclear Instruments and Methods*

Operated by Universities Research Association Inc. under Contract No. DE-AC02-76CHO3000 with the United States Department of Energy

Disclaimer

R & D on Mechanical Construction and Cooling of a 3-D Silicon Vertex Detector

Paul Lebrun, Carl Lindenmeyer,
Linda Stutte, Herman Cease*
and Dan Chissus

Fermi National Accelerator Laboratory†
P. O. Box 500, Batavia, IL 60510

Abstract

This paper presents results on mechanical and cooling studies for a 3D silicon vertex detector designed for B physics at a hadron collider. Prototype modules were built from raw silicon wafers. One module was instrumented with resistors to simulate readout electronics. A cooling method utilizing simple air/helium flow was investigated. Both module movement and temperature variations were recorded.

---

*Present address: Northern Illinois University.

†Work supported by the U.S. Department of Energy under contract NO. DE - AC02 - 76CHO3000

1 Introduction

As stated on numerous occasions, a silicon vertex detector (SVD) designed for B physics in a hadron collider environment is, by necessity, ambitious and complex[1][3]. In such vertex detectors, the position of the silicon wafers must be known and kept stable with an accuracy of a few microns, while the electronic readout dissipates heat at close proximity. The mechanical and cooling studies described in this work are now recognised to be as crucial as developments in VLSI electronics.

This paper is organised as follows. In the first section, requirements and tradeoffs for a 3D vertex detector are discussed. The second section describes the experimental setup, including the construction of modules, the placement of these modules in a rigid support assembly, and the instrumentation used to measure the motions and temperatures of individual wafers. The third section presents results on air and helium cooling.

2 Requirements and Conceptual Design of a 3D Vertex Detector

Requirements leading to the basic BCD design have been studied with Monte-Carlo simulations and subsequent analysis [2]. In order to have good separa-

tion between bottom- or charm-vertices and the primary interaction vertex, one must have a spatial resolution for these vertices on the order of 20 to 40 μm. This can be achieved with a set of 25 μm pitch silicon detectors placed at a distance of a few cm from the interaction point. Particle coordinates must be measured in at least two stereoscopic views to accurately reconstruct the vertices in three dimensions. At least 3 positions per track must be recorded. The vertex detector effective acceptance must obviously match the acceptance of the other elements of the spectrometer. In order to accurately measure the CP violation amplitudes in difficult decay modes of the B-meson, such as $B^0 \rightarrow \pi^+\pi^-$, at the Tevatron collider this acceptance must cover at least ± 2 to 3 units of pseudo-rapidity. This corresponds to track angles ranging from a few degrees away from the beam up to 90°. Limitations on position resolution at the wafer as the tracks cross the detector plane at a grazing angle lead to a design in which silicon wafers are both parallel to the beam (Barrels) *and* perpendicular to the beam (Disks). In order to control pattern recognition failures while reconstructing complex decays such as $B \rightarrow D \rightarrow$ kaons buried within high multiplicity events, the strip length must be limited to a few cm. Because the luminous region along the beam direction extends over approximately 30 to 50 cm, the Disk and Barrel wafers must be interleaved.

These considerations led the BCD collaboration to a conceptual design shown in Figure 1. A module consists of three layers of Barrel type wafers (6 Inner, 6 Middle and 12 Outer wafers), and two planes of Disk type wafers (6 Inner and 12 Outer wafers). These modules are hexagonally shaped, approximately 10 cm in radius and 4 cm in length (see Figure 2) . About 10 modules are held in place in a long rigid gutter by a set of kinematic supports.

The BCD design described here is technically more demanding than the CDF SVX II detector[23], which has only Barrel type wafers, characterised by a maximum strip length of approximately 17 cm. The D0 collaboration is currently working on a design involving disks and barrels, avoiding the problem of interleaving them[24]. These solutions are certainly easier, but will de-facto limit the effective acceptance of the detector.

The last and probably most crucial consideration in an SVD design is the mass of the detector. Electron pair creation, hadronic interactions and multiple scattering significantly affect the performance of such a detector. For instance, a 200 μm thick silicon plane will deflect a track of momentum P (in GeV/c) on average by an angle of

$$\theta_{rms} \approx 0.65 \times 10^{-3}/P.$$

A deflection of a few mrad significantly degrades the track position resolu-

tion at the vertices. Thus, the amount of mass which contributes to multiple scattering must be severely limited. Support structures, cooling elements and electronic readout components must be of mass comparable to that of the detectors. A very low mass design can be achieved based on the following features:

- The silicon wafers are almost *self supporting.* In this design, the passive structural elements supporting the wafers are tiny glass prisms, the kinematic mounts and a thin web to insure the gutter's rigidity. (Note that the tracks are measured in at least 2 to 3 planes before they hit these last two supporting elements.)

- The detector is air or helium cooled. No pipes are necessary, no additional mass is required.

- The electronic readout is highly integrated to the detector: VLSI technology is an absolute must. Pre-amplifiers, discriminators, amplifiers and digitizers are on a single chip, placed on a Data Collection Bus (DCB) glued on the wafer itself.

- Short, light cables bring the data collected by individual wafers to a Data Collection Chip (DCC) located outside the module, probably within the gutter. A second set of cables connects the DCCs to the

data acquisition system.

This work concentrates mainly on the first two items in this list. Module prototypes have been built using a *semi-hand* assembly technique described below. A simple rigid gutter hosting as many as four modules has been used to test the air or helium cooling method. VLSI R&D has been addressed elsewhere[5] and will not be discussed here. Let us simply mention that a CMOS chip capable of reading 128 channels, sized at approximately 1 cm^2, could be designed and built. The power consumption would be at least 1 mW per channel. As we plan to read out every other channel across the 25 μm pitch wafer, the typical power consumption across the DCB is roughly 0.2 W/cm. The total power requirement for a module is about 100 W.

3 Description of the Apparatus

3.1 Overview

In order to study the mechanical and thermal properties of this detector, one obviously does not need to use active silicon wafers. Our prototypes were made using raw silicon wafers. The electronic readout was simulated by a simple set of surface mount resistors, which provided a tunable heat load on the detector. Instrumentation included capacitive probes to measure wafer

motions and thin film detectors (TFDs) to measure temperature changes. As this study concentrates mainly on the SVD detector itself and not its integration into the full collider detector, the modules could be placed in a minimal gutter, where mechanical rigidity is reached by simply constructing it with thick plates. Finally a closed- or open-loop ventilation system capable of circulating air and a tunable air/helium mixture has been installed. These elements are reviewed in more detail below.

3.2 Selection and Preparation of the Silicon Wafers

Industry standard silicon wafers were used[6]. These 4" diameter wafers had a nominal thickness of 250 μm, with a tolerance of 25 μm. The crystal type was { 100 }: we verified that the fracture orientations had the 4-fold square symmetry characteristic of this crystal orientation. These wafers were laser cut[7] into rectangular or hexagonally shaped pieces described in Figure 2. Cuts were made along the { 100 } direction, except for the 60° angle side of the Disk type wafers. The Inner Disk type wafers were particularly sensitive to breakage along the 60° symmetry axis. Tolerance on these cuts was of the order of 50 μm. Flatness was also an important consideration, as stress induced fractures occur when bowed wafers are forced into the module. Wafers with a bow greater than $\approx$ 100 μm over a few cm were not used for

this type of assembly.

Attempts were made to measure stress prior to possible crystal fracture. Unfortunately, no adequate method was found. Brittle paint[8] was too coarse. Strain gauges work only on small areas of the wafers. Adequate sensitivity could not be reached with the Photoelasticity method[10]. As the module assembly method and procedures improved, no fractures due to mechanical stress were observed. Therefore no other methods to quantitatively control stress on the wafer were tried.

3.3 SVD Module Assembly

Wafers are held together in a module by small ($\approx$ 1 mm in width and a few mm in length) glass pieces, shaped as triangular prisms for the Disk/Barrel connections and as rectangular 60° chevrons for the Barrel/Barrel connections[9]. These small pieces are directly glued onto the wafers. The mechanical robustness of these tiny glue joints was found adequate, as the wafer breaks before the glue joint does[4]. The chemical properties of the glue do not affect the electrical properties of a real working silicon detector[4]. In addition, in this design, an aluminum nitride board which supports the electronic readout components must be glued onto the wafer. The room temperature coefficients of linear thermal expansion of these structural materials are almost

identical: $2.6 10^{-6} K^{-1}$, $2.5 10^{-6} K^{-1}$, and $2.8 10^{-6} K^{-1}$, for silicon, aluminum nitride and pyrex, respectively. Thus, the entire module assembly is expected to be robust against temperature variations. Several silicon-glue-glass prism assemblies have been temperature cycled between $-20°C$ to $60°C$ without damage. Modules were assembled *semi-manually*, using a set of temporary fixtures and supports to position and hold the wafers in place prior to gluing. Three types of supports were used: (i) a fixed hexagonal mandrel to hold a module by its core while wafers were added, one at a time; (ii) alignment supports which allowed an accurate positioning of the wafers; and(iii) a movable fixture (the carrier) which was used to transport a given wafer from the alignment support to the mandrel fixture. Obviously, the 6 Inner Barrel wafers were positioned first, the 12 Outer Barrel wafers last. Precision pins were used to align the carrier with either the alignment support or the mandrel (see Figure 3). To insure proper behavior under thermal stress, wafers were not allowed to touch each other. A 50 μm thick temporary shim was inserted in all cracks separating the wafers. Minor corrections to the alignment could be made prior to gluing.

As mentioned previously, these modules can easily be equipped with *simulated readout*, in order to study the cooling requirements. On each individual wafer, prior to assembly, a small (0.9 mm in width by a few cm in length)

aluminum nitride board was glued on the wafer, one on each side, near the edge of the wafer. Surface mount resistors were mounted on this board, simulating the VLSI readout chips. This simple electronics was able to dissipate up to 0.4 W/cm along the board, corresponding to roughly 2 mW per channel assuming a 50 μm pitch readout system.

In this assembly, wafers were positioned and held in place in the structure with an accuracy on the order of 50 to 100 μm. This accuracy is limited in part by the precision pin fittings and by fluctuations in wafer size. Five modules were built using this technique, one of them equipped with simulated readout. Although the first module had a few broken wafers at the end of the assembly procedure due to various mishandlings, the last few of them had no breakage or other defects. Nevertheless, a robotic assembly procedure is required not only for accuracy but, as important, for quality control and yield[11]. This work is currently in progress[12].

Silicon modules and the gutter supporting these modules have different coefficients of thermal expansion. A set of classical 3-point kinematic mounts located around the module has been designed to handle mechanical stress occuring upon a temperature change. These 3 brass mounts lie in a plane oriented perpendicular to the beam direction. All of these modules were built at room temperature, mounted on their kinematic mounts, and inserted in

the gutter. This assembly (containing a module) has been cooled to $-24°C$, and brought back to room temperature without mechanical damage. Modules returned to their original position within an accuracy of 10 μm. In this application, we have made use of an interesting property of silicon crystals: namely, that their structure is diamond like, and this implies that the coefficient of thermal expansion is the same for all crystal axes. Hence, the expansion or contraction of the entire module occurs isotropically, causing no damaging stress to the module.

3.4 Signal Cable Prototypes

Early prototypes pointed out the need to have a multiplexing arrangement for the cables. Without this, one would be faced with the problem of routing 84 cables/module (times 10 modules) to a remote data collection site. Also, by making the cables shorter, they can then be thinner and thus present less mass to transitting particles. Prototyping has shown that we can build a 24-conductor cable, less than 100 μm thick (corresponding to a total 0.3 % radiation length), roughly 1/4 in wide and a foot long with adequate electrical properties to carry the signal from the inside of the module to a Data Collection Chip glued on the outer face of the module. In order to carry the power for the simulated readout chips, similar cables made of mylar

insulator and two flat copper foils were assembled and have been installed onto the instrumented module, as shown in Figure 4.

3.5 Description of the Position Sensors

Wafer or module motions must be recorded with an accuracy better than the intrinsic silicon vertex resolution, i.e., on the order of a few microns or better. In order to avoid stress on the module, no direct mechanical couplings between the module and the position sensors are allowed. Optical systems can be very accurate, but are expensive and difficult to use in a complicated geometry. Based on cost and spatial and mechanical constraints, a non-intrusive, capacitive method commercially available[13] was selected. Such systems have been used previously in colliding beam detectors[14].

A measurement of the electrical capacitance between a target plate and a sensing plate can easily be converted to a relative distance between these two elements. The capacitance is measured with the use of a constant ac current source of a precisely controlled frequency (around 15 KHz) and a low capacitance voltage pre-amplifier that measures the voltage drop across the target/sensor gap. In order to further reduce cost and to facilitate mechanical integration into our gutter assembly, the sensors were built in-house. The capacitive sensors were assembled as follows: The body of a female Lemo

barrel connector[15] serves as the guard ring. The signal pin is capped with a brass "button" serving as the sensor capacitive plane, as shown in Figure 5. The sensing surface was approximately 0.124 cm^2. The button is held in place and insulated from the body with standard epoxy glue. This assembly is then ground flat, polished and mounted in a grounded cylindrical support attached either to the calibration setup or inside/outside the gutter. The probes were connected to the amplifier inputs with RG188 coaxial cables. These low-noise teflon-coated cables were thin, flexible and could sustain cold temperatures.

All sensor/amplifiers used in this experiment have been carefully calibrated. The distance between the probe and the sensor was measured independently with a micrometer. As shown in Figure 6, these probes are linear over an acceptable range of 50 μm to 2 mm. In most cases, these probes are best used when the sensor plane is parallel to the target plane, thus measuring a distance perpendicular to this plane. If the sensor surface does not entirely cover the target plane, the probe also becomes sensitive to motion parallel to this plane, as the capacity is proportional to the effective surface. In such a configuration, it is obviously not possible to decouple both motions at a given location. Since the motion direction of a module or an individual wafer is hard to predict in our geometry, our sensors always covered the

target surface, insuring the uniqueness of the motion direction.

Up to 16 probes have been installed around modules in the aluminum gutter, monitoring motions of up to two modules along the beam axis, with a relative accuracy of a few microns (and an absolute accuracy of 50 to 100 μm). These probes have also been installed around the hexagonal shaped sides of the gutter, monitoring motions perpendicular to the beam.

3.6 Temperature Sensors

In addition to silicon modules and position sensors, the gutter assembly was also equipped with thermometers of the type TFD (thin film detectors)[16] characterised by small physical size (0.3 cm^2), a large surface area to volume ratio and good thermal conductivity between the substrate and the sensor. The relative(absolute) accuracy of such devices is $0.50°C$(a few degrees). The TFDs were either suspended in the volume in order to measure the bulk gas temperature, or glued directly onto the wafers of the intrumented module. The gutter body temperature was also monitored.

3.7 Gutter Assembly, Closed Ventilation Loop

The gutter assembly was connected to a closed loop or open ventilation system consisting of a regenerative blower[18], a long straight section in which

the laminar gas flow was measured and an optional cooling box to stabilise the gas temperature. The total volume of the system was approximately 0.26 m^3. The air flow was measured with a set of general purpose air velocity transducers[17]. For the helium measurement, these devices were independently calibrated, using mass flow gravity gauges. When helium was used, the air to helium mix was measured with an oxygen sensor characterised by a range of 0.5% to 21.0%[19].

In order to have good cooling efficiency, a set of guides made of aluminum and foam materials were inserted inside the gutter, upstream of the modules. These guides distribute the air flow across the Disk faces of the most upstream module, and prevent gas from escaping around the modules. Thus, most of the volume flow occurs within the inside helicoidal paths (Inner Disk and Outer Disk), from one module to the next.

3.8 Data Acquisition

A Macintosh IIcx connected to a Keithley 705 Scanner through a standard GPIB interface allowed us to monitor up to 40 different voltages at a time. Temperatures, wafer positions and air velocities can be monitored for extended periods of time. LabView II[20] was used both for data acquisition and display/analysis.

4 Results on Air and Helium Cooling

To maximize cooling power while avoiding mechanical damage, up to 60 gm/sec of air or 7 gm/sec of helium were circulated in the system. The air moves across a module, or from one module to the next through openings surrounding the beam axis and parallel to it. The total surface available for flow is on the order of 30 cm^2. Thus, the Reynolds number is at least on the order of 5.4×10^4 for air, and 7.4×10^3 for helium. In either case, this crude estimation indicates a turbulent flow. Turbulence has been qualitatively observed at the exhaust locations, a few mm downstream of the last module. A turbulent regime enhances the heat transfer rate, especially when the flow is not fully developed in this complicated air duct.

The pressure drop across a module is small, on the order of 0.4 cm of water, or less. Thus, to a good approximation, the entire detector runs at atmospheric pressure. Yet, because of the small thickness and weight of the silicon wafers, significant motions have been observed as the air circulates. One can distinguish between three types of module or wafer motion:

- *Bulk motion.* Wafers or modules are mostly moving along the beam axis as the gas flow applies pressure along that direction. Outer Barrel

wafer motions are only of the order of a few microns or less upon turn on of the gas flow, while the center of an Inner Disk wafer in the most upstream module, upstream face, moves as much as 90 μm along the beam direction. (Motions of the downstream faces are smaller.)

- *Motion due to temperature variation.* Heat is produced either by power dissipation from the similated electronics on the modules themselves or by the gas compression occuring in the blower. Although exact motions are hard to predict as the modules dilate in this complicated geometry, one expects typical motion only on the order of 0.05 to 0.10 μm per $^{\circ}C$ within a module. Module motions due to distortions of the aluminum gutter are much bigger, of the order of 1 to 2 μm per $^{\circ}C$. The reaction of the module to this mechanical stress through the kinematic mounts is, if not predictable, reproducible. As the temperature cycles between $20^{\circ}C$ to $-24^{\circ}C$, wafer or module motions of the order of 30 to 40 μm have been observed (see Figure 8). At constant temperature, the system remained stable despite the turbulent gas flow. Wafer positions have been monitored for hours, and only minor motions (less than a few μm) were observed. These were compatible with small temperature changes (less than a few $^{\circ}C$).

- *Vibrations.* Once again, for simple geometries, vibration properties are

calculable[21]; a $5cm \times 5cm$ square wafer is expected to vibrate with a characteristic frequency of $\approx$ 160 Hz. In our geometry, a broader range of frequencies is expected. These vibrations were observed with the same capacitive motion sensors, as the amplifiers have good linear response for such low frequencies. A dynamic signal analyzer was used to measure frequencies and amplitudes, presented in Figure 9. Because of the broad distribution of frequencies, these vibrations are de-facto chaotic motions of the wafers. Although the average deviations are only on the order of one micron, instantaneous excursions from the equilibrium position could easily reach 6 μm, at a near maximum gas flow rate of 50 gm/sec. As in bulk motion, these vibrations are more important for the Disk wafers of the most upstream module. Replacing air by helium at a fixed volumetric flow does not reduce the amplitude of these vibrations.

4.1 Temperature Distributions

The temperature within and around the modules has been measured versus heat load created by the simulated readout electronics, versus gas flow and versus location across the module. Figure 10 shows a typical measurement cycle, in which the stable system is heated, reaches thermal equilibrium and

then cools down once the electronics is turned off. The temperature elevation ΔT is defined as the difference between the two thermal equilibria, with/without power on the simulated readout system. ΔTs are always directly proportional to the heat load (see figure 11). Typical elevations are on the order of $\approx 0.15°CW^{-1}$, at maximum gas flow. The bulk temperature elevation of the gas, measured a few cm downstream of the module is smaller, on the order of 0.04 to 0.08 $°CW^{-1}$, as expected: the turbulent gas can not be in thermal equilibrium with the wafers.

ΔT has been also measured as a function of gas flow, shown in Figure 12 for pure air, and as a function of the mix ratio of air to helium at a given volumetric flow in Figure 13. (As the gas density changes, the blower is unable to keep this volumetric flow strictly constant; data in Figure 13 have been corrected for this small effect.) As the flow increases, so does the inefficiency of the cooling: ΔT does not decrease linearly with the flow. This is expected, based on a simple energy conservation law. (See Figure 12 for a theoretical comparison.)

Finally, temperature elevations have been measured on the module at many locations, as this system is not expected to be isothermal. The z dependence of temperature elevation is given in Figure 14. As expected, the temperature rises with increasing depth through the helicoidal paths within

the module. A more detailed radial scan presented in Figure 15 shows that the heat transfer between the aluminum nitride board and the silicon is quite good: the board is almost in thermal equilibrium with the wafer.

5 Conclusions

A realistic mock-up of a large acceptance 3D silicon vertex detector has been built and used to test a cooling method based on a forced air (or helium) circulation. The construction of the prototype modules was successful. It has been demonstrated that low-mass supports can be used to assemble a 3D silicon vertex detector.

However, the cooling method investigated here is not likely to work in a final design: at a load of 100 W per module, temperature anisotropies within a module will be of the order of 10 to 15°C and an increase of up to 20°C from one module to the next one is expected. An overall temperature increase of $\approx$ 50 to 100°C in a complete system will impose too much thermal stress on this type of structure, and the electronic readout is not expected to work in this temperature range. Existing detectors are currently working with a temperature anisotropy of $\approx$ 5°C[27]. Increasing the gas flow does not pay off, as the cooling efficiency decreases and the already worrisome vibrations will increase. Because of their complex and chaotic behavior, these

vibrations can not be corrected for in software. Damping them through adhoc mechanical means would imply an intolerable increase in mass.

Thus, a more efficient cooling method needs to be investigated. Although the heat transfer between the readout electronics and the wafers is adequate, forced air convection is not good enough to cool the structure. A solution employing multiple air vents instead of a continous helicoidal path is difficult to achieve without loosing geometrical acceptance. In essence, one needs to find a mechanism to cool the gas *within the modules* themselves and not outside the gutter assembly. A method based on evaporative cooling, in which a liquid of high latent heat of vaporisation flows into the detectors and evaporates has been proposed[25][26]. This method is currently under investigation.

6 Acknowledgements

We wish to thank the Fermilab Physics Department for their generous support during these tests. We especially want to recognize Jorge Montes for his meticulous attention to detail in the construction of the SVD modules. We also want to thank Paul Ratzmann from the Fermilab Research Division Mechanical Department for good advice about and calculations for cooling systems.

References

[1] H. Castro *et al, Proposal for Research and Development: Vertexing, Tracking and Data Acquisition for the Bottom Collider Detector*, submitted to the Fermilab PAC (January 2,1989).

[2] P. Lebrun, *A Bottom Collider Vertex Detector Design, Monte-Carlo Simulation and Analysis Package*, Fermilab TM-1682.

[3] N. Lockyer *et al, Proposal for a B-Physics Experiment at TeV I - The μBCD*, submitted to the Fermilab PAC (October 8,1990).

[4] H. Cease, *Adhesive Tests for Use on 3-D Silicon Vertex Detectors*, Fermilab-Pub-91/353.

[5] T. Zimmerman, M. Sarraj, R. Yarema,*Design of an Advanced Readout Chip for Silicon Strip Detectors*, to be published in the Proceedings of the Nuclear Science Symposium, 1992.

[6] Supplied by Aptek Corporation.

[7] Supplied by LaserAge Corporation.

[8] Supplied by Electrix Industries.

[9] Supplied by Newport Glass Works, Inc.

[10] Private communication, Fermilab Technical Support.

[11] Carl Lindenmeyer, *Proposed Method of Assembly for the BCD Silicon Strip Vertex Detector Modules*, Fermilab TM-1627, (1989).

[12] Hans Jöstlein, H. Cease, private communication.

[13] Amplifier Model 410S, supplied by Capacitec Inc.

[14] A. Breakstone et al., Nucl.Instr.and Meth. A281, p 453-461,(1989).

[15] Part # 1079-5, supplied by Kings, Inc.

[16] Supplied by Omega Technology Company.

[17] Type FMA-6000, supplied by Omega Technology Company.

[18] Supplied by Hans Jöstlein, private stock.

[19] Supplied by Snap-On Tools Corp., Model # MT1185.

[20] Supplied by National Instrument Co.

[21] See for instance, S. Timoshenko and S. Woinowsky-Krieger, *Theory of Shells and Plates*, McGraw-Hill Book Company, 1959.

[22] Supplied by Hewlett Packard Corp.

[23] M. Gold, *CDF Upgrade Capability*, talk presented at the B Physics at Hadron Accelerators Workshop, Nov. 16, 1992.

[24] A. Heinson, *The D0 Upgrade Silicon Tracker*, talk presented at DPF92. Nov. 13, 1992.

[25] W. O. Miller *et al*, *Superconducting Super Collider Silicon Tracking Subsystem R&D*, Los Alamos note # LA-12029,(1990).

[26] SDC Collaboration, *Silicon Tracking Conceptual Design Report*, SDC note # SDC-91-133,(1991).

[27] Private communication: F. Rafaelli.

Figure Captions

1. The reference design of the BCD vertex detector is shown in this drawing. The hexagonal shaped modules surrounding the beam pipe are located in a beryllium gutter.

2. Description of the module geometry. Five distinct wafer types have to be inserted into the hexagonal structure: from inner to outer, Inner Barrels, Inner Disks, Middle Barrels, Outer Disks and Outer Barrels.

3. A photograph of the module assembly, showing the fixed central mandrel supporting the module while the carrier is holding an Outer Disk while it is being glued onto the Middle Barrel.

4. A photograph of the instrumented module mounted inside the aluminum gutter. Two kinematic mounts (top and bottom), Outer, Inner disks and Barrel type wafers, Mock-up of the Data Collection boards (located on the outside of the outermost barrel wafers), aluminium nitride boards glued directly onto the wafers (with small resistors mounted perpendicular to their length) and position sensors mounted in brass tubes are visible in this picture.

The flexible, flat copper cables are mock-ups of signal/power cables. The white cables are for the temperature sensors.

5. Engineering note on the construction of a capacitive Lemo probe. Only the left hand side of the connector is modified.

6. A typical position sensor calibration curve, showing good linearity for distances up to $\approx$ 2 mm.

7. Motion of the Disk wafers as a function of gas flow. The position sensor was targeting the most upstream Inner Disk in the system.

8. Longitudinal motion due to temperature change. In the left graphs, the gutter (dotted) and gas (continuous) temperatures. (The top continuous line indicates the room temperature). On the right, a typical variation of the distance between a wafer (Inner disk) and the position sensor rigidly mounted on the Aluminium gutter.

9. Oscilloscope display showing the frequency distribution of wafer vibrations (upper graph) and the chaotic motions (bottom curve). One mV corresponds to approximately 3 μm. The position sensor was targeting the most upstream Inner Disk in the system.

10. A typical temperature measurement cycle, at constant gas flow. The arrows indicate the time at which the power (30 Watts) was

turned on and off.

11. Temperature elevation versus power dissipated by the instrumented module. The air flow was approximatly 50 gm/sec. Triangles refer to a typical Outer Disk, circles to a Inner Disk.

12. Temperature elevations measured for 40 Watts of dissipated power. The triangles and circles refer to the same points on the module as in the previous figure. The squares are the temperature elevation of the air in the vicinity of the module. The curve is an simple estimate of this elevation assuming energy conservation.

13. Temperature elevation measured on the hottest Aluminium Nitride board (triangle) and on the corresponding wafer, at approximatly 1 cm distance, versus the helium volumetric concentration at almost a constant volumetric flow. This flow rate at 0% helium was 52 gr/sec. The dissipated power was 30 Watts.

14. Based on data presented in the previous figure, temperature elevations are shown as a function of the longitudinal distances between the thermometers and the center of the module. As expected, a strong increase is observed as one moves from upstream to downstream in the gas flow.

15. Based on a different set of data then previous figures, temperature elevations are shown as a function of the radial distance between the center of the module and the thermometer, showing little variation across the wafer. The arrows indicate the location of the Aluminium Nitrde board glued onto the wafer. The circles refer to a Disk located about 1 cm upstream of the most downstream disks (triangles). The air flow was about 55 gr/sec, the dissipated power was 30 Watts.

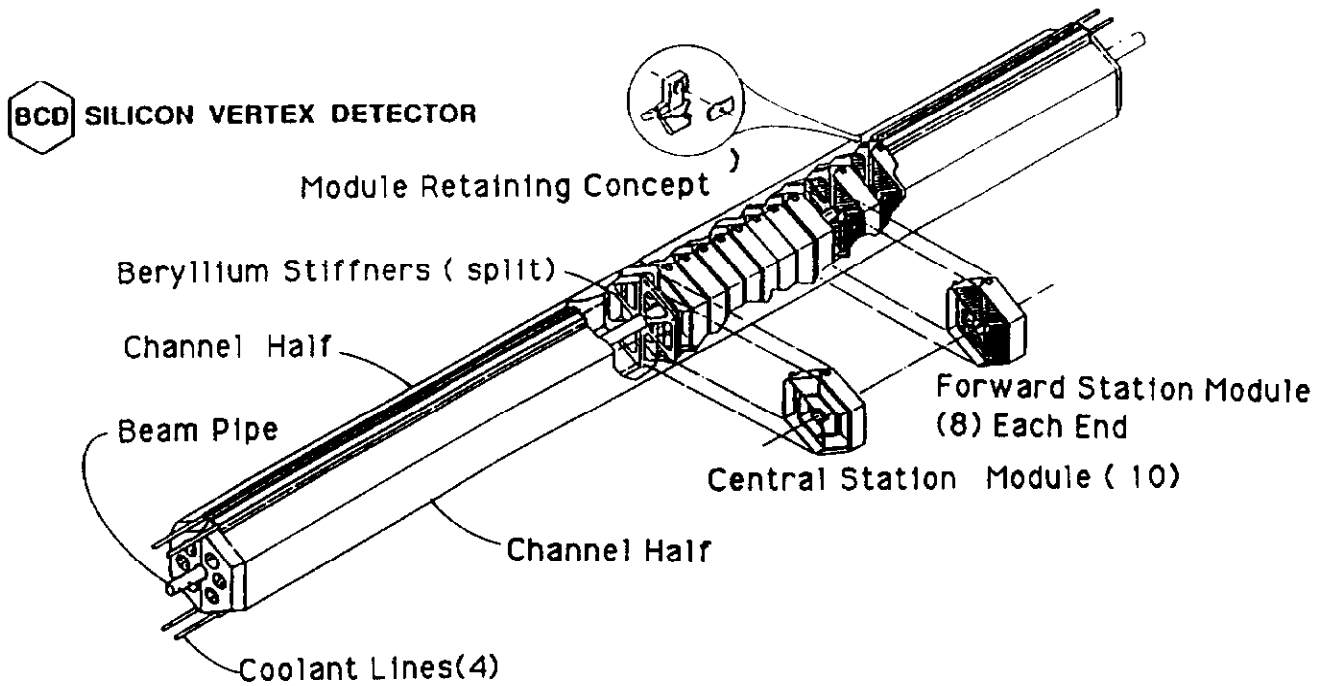
BCD SILICON VERTEX DETECTOR
Module Retaining Concept
Beryllium Stiffners (split)
Channel Half
Beam Pipe
Forward Station Module
(8) Each End
Central Station Module (10)
Channel Half
Coolant Lines(4)

Figure 1

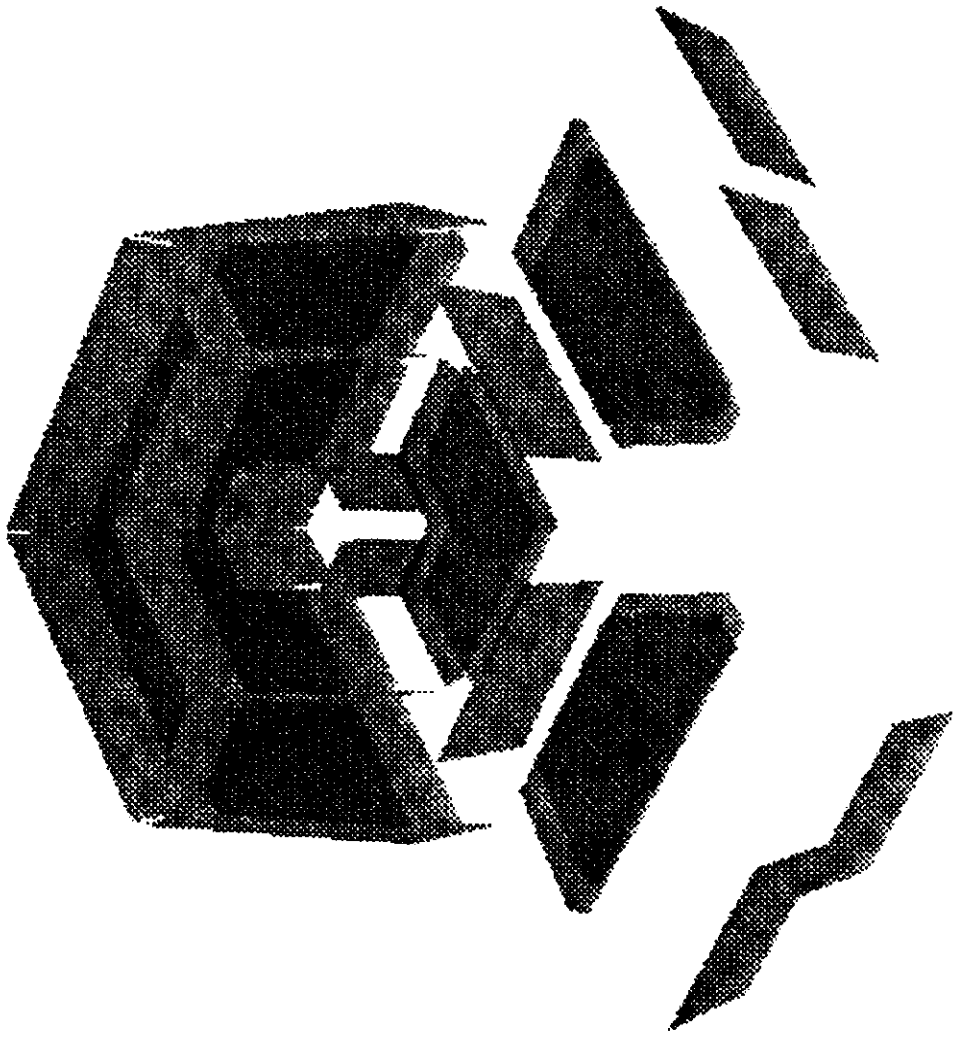

Figure 2

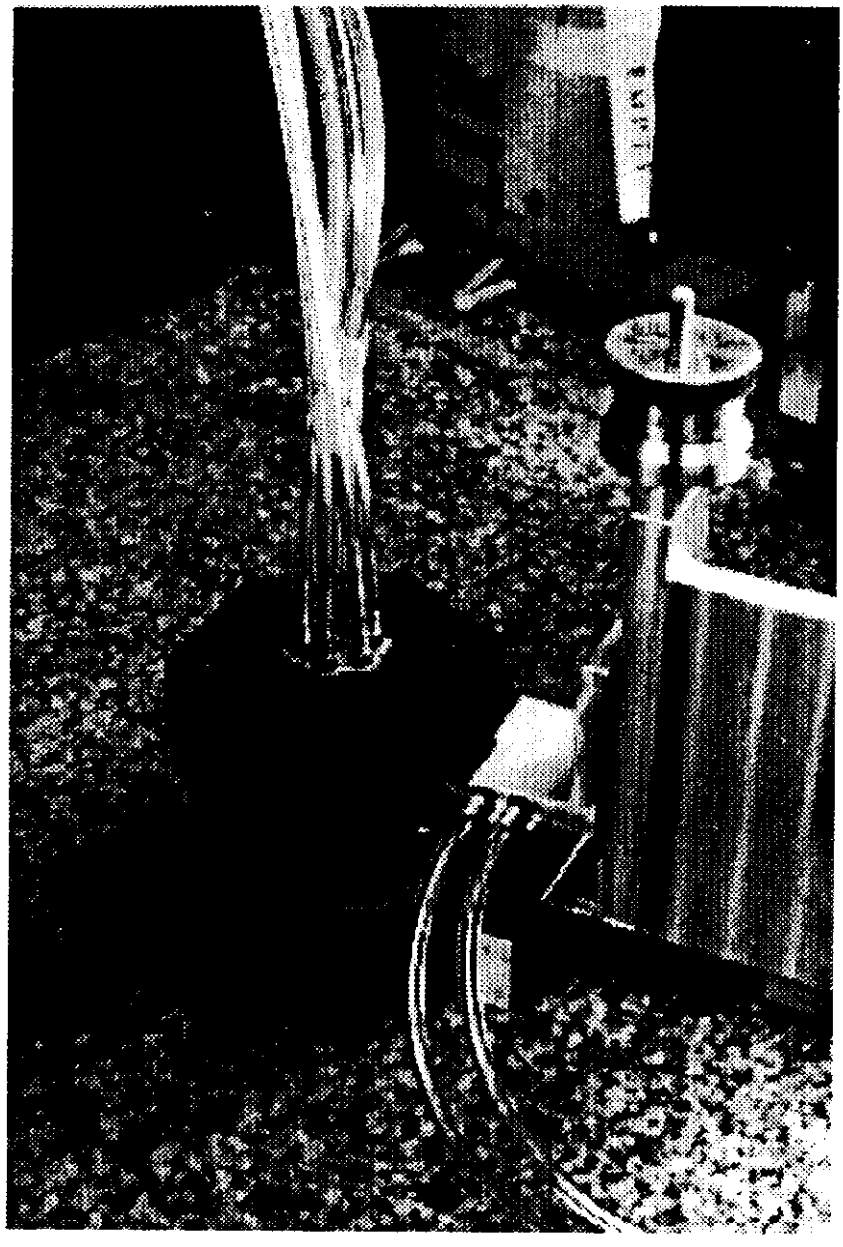

Figure 3

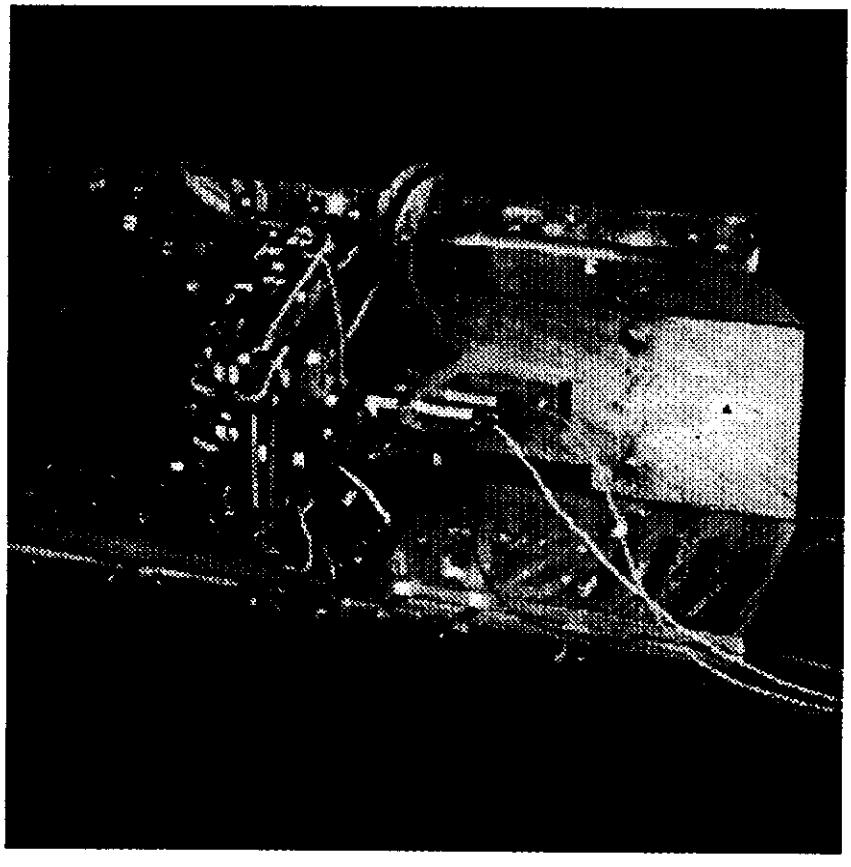

Figure 4

Capacitive Probe Constructed from a King's #1079 Connector

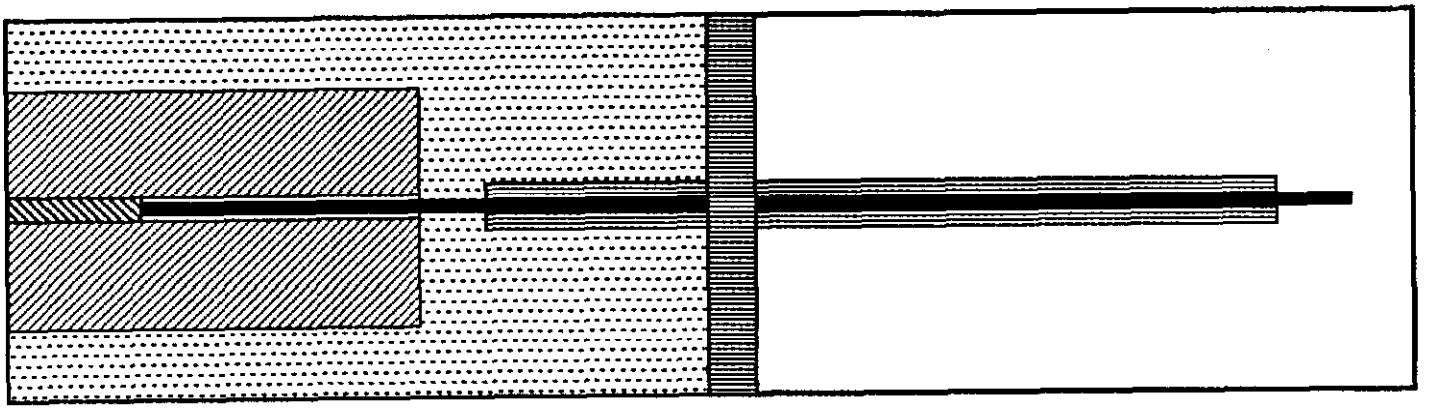


Solder


Brass Pin


Plastic Insulator

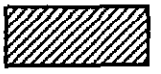
Brass Sensor

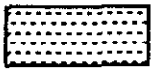
Epoxy

Figure 5

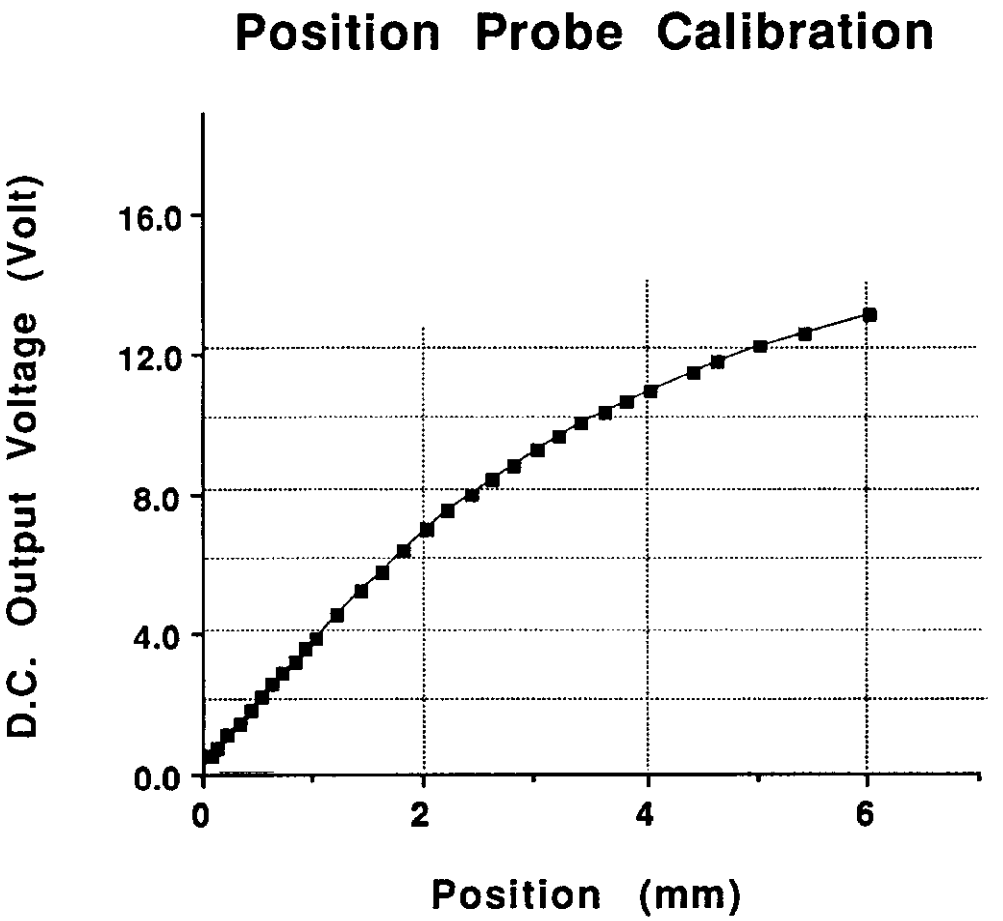
Position Probe Calibration
D.C. Output Voltage (Volt)
16.0
12.0
8.0
4.0
0.0
0
2
4
6
Position (mm)

Figure 6

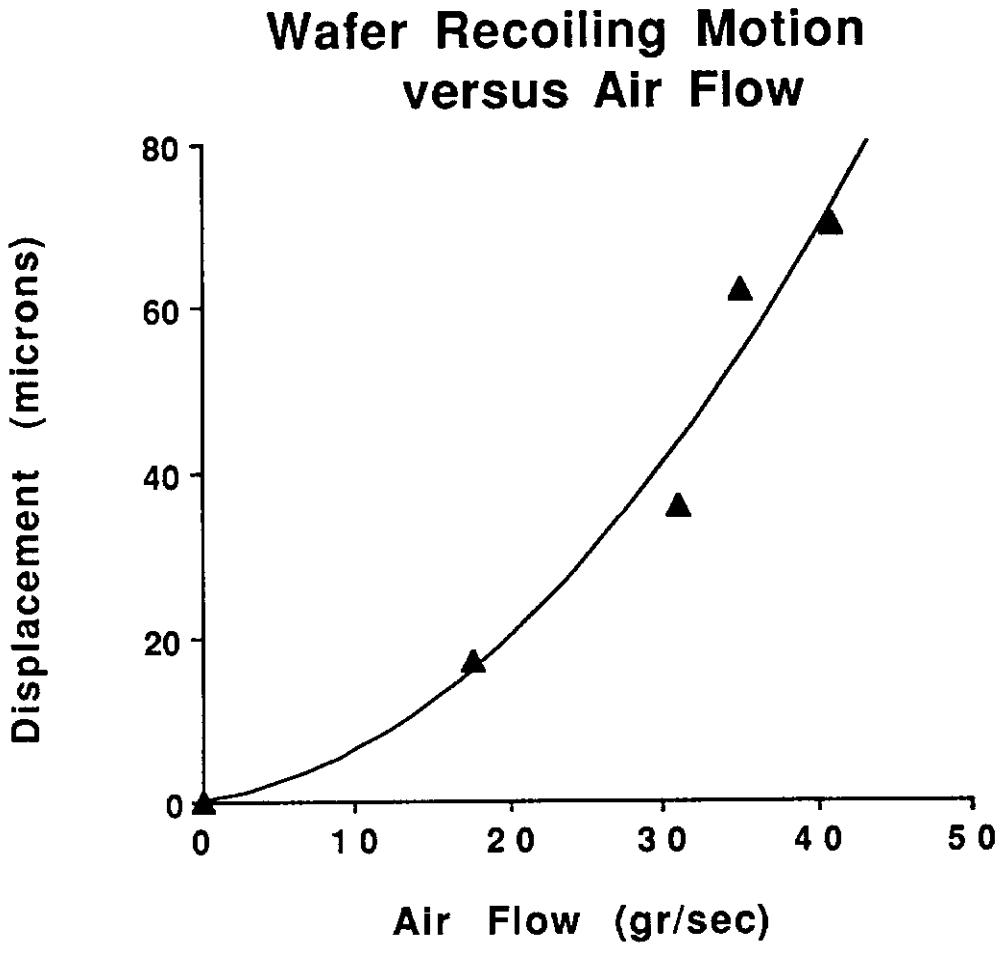
Wafer Recoiling Motion
versus Air Flow
Displacement (microns)
80
60
40
20
0
0
10
20
30
40
50
Air Flow (gr/sec)

Figure 7

Temperature and Wafer Position versus Time

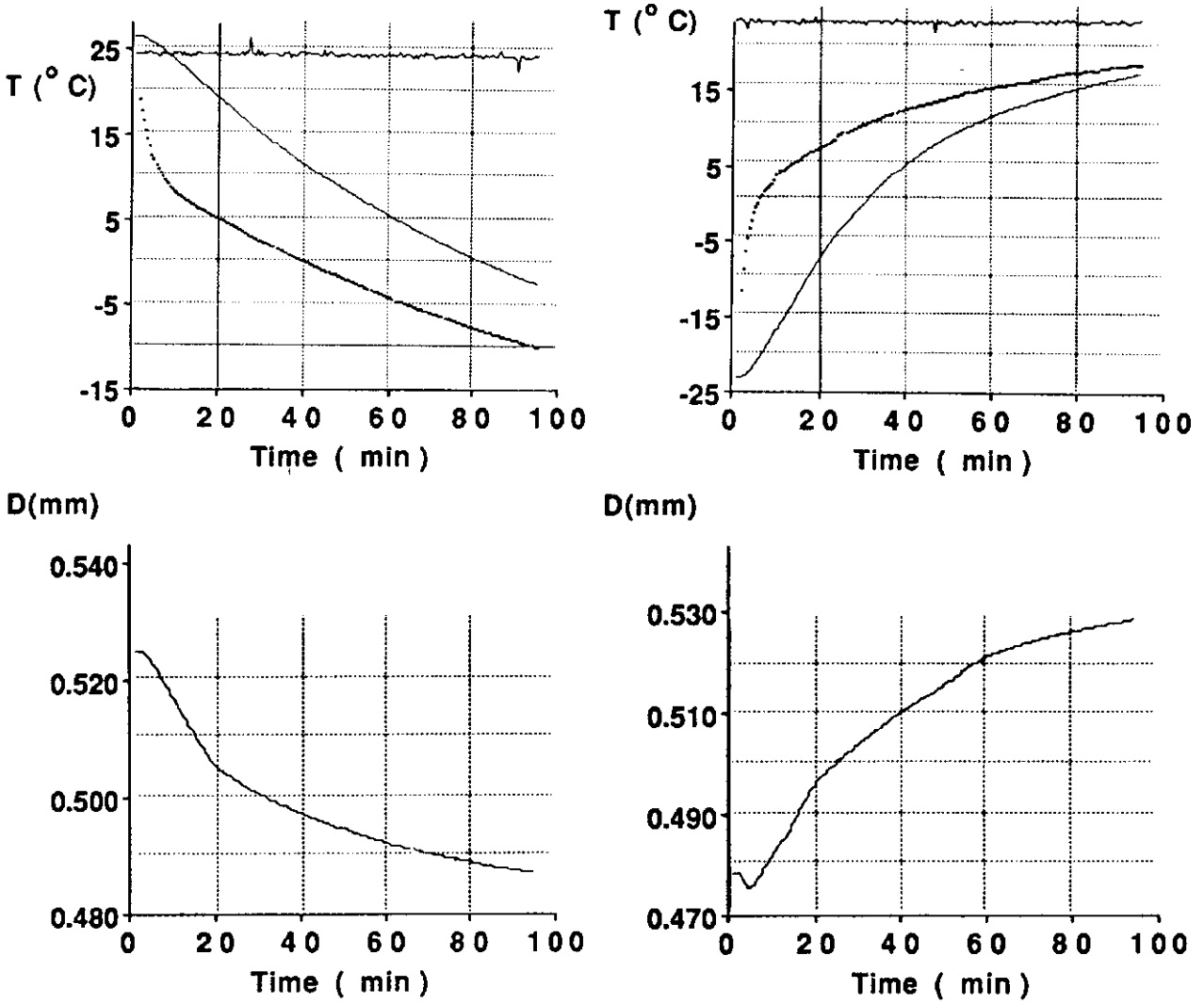

Figure 8

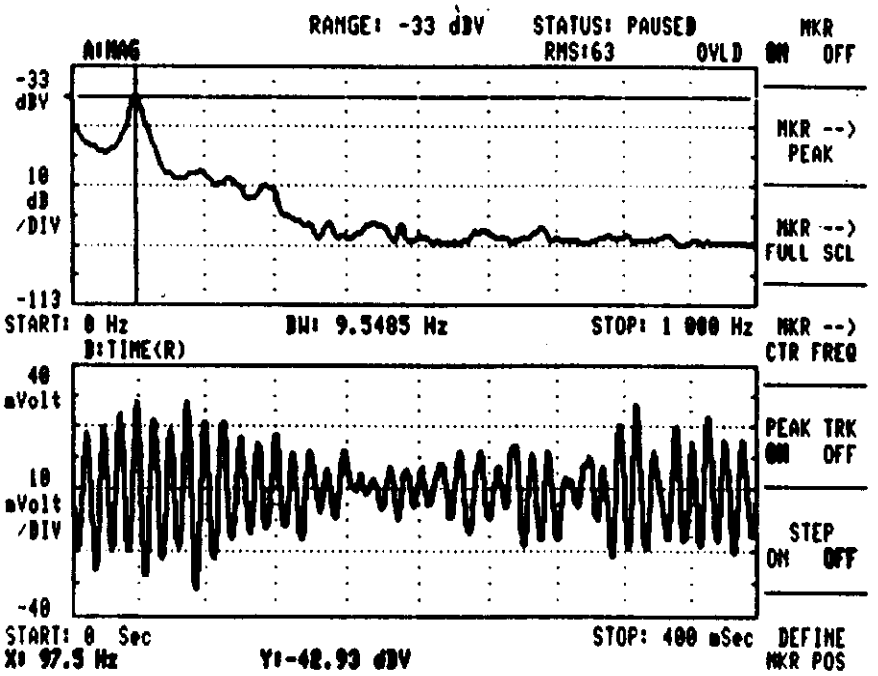
RANGE: -33 dBV
STATUS: PAUSED
RMS:63
OVLD
MKR
ON OFF
A:MAG
-33
dBV
10
dB
/DIV
-113
MKR --)
PEAK
MKR --)
FULL SCL
START: 0 Hz
BW: 9.5485 Hz
STOP: 1 000 Hz
MKR --)
CTR FREQ
B:TIME(R)
40
mVolt
10
mVolt
/DIV
-40
PEAK TRK
ON OFF
STEP
ON OFF
START: 0 Sec
STOP: 400 mSec
DEFINE
MKR POS
X: 97.5 Hz
Y: -48.93 dBV

Figure 9

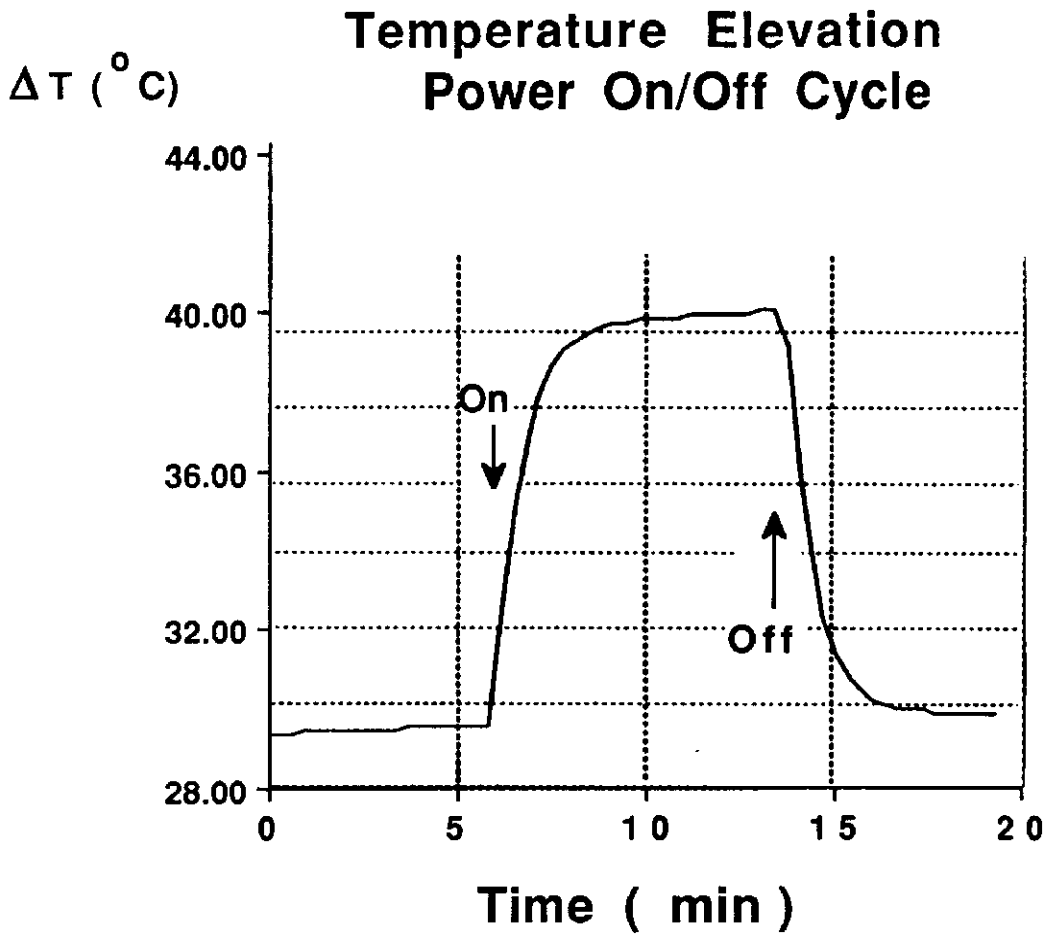
Temperature Elevation
Power On/Off Cycle
ΔT (°C)
44.00
40.00
36.00
32.00
28.00
On
Off
0
5
10
15
20
Time (min)

Figure 10

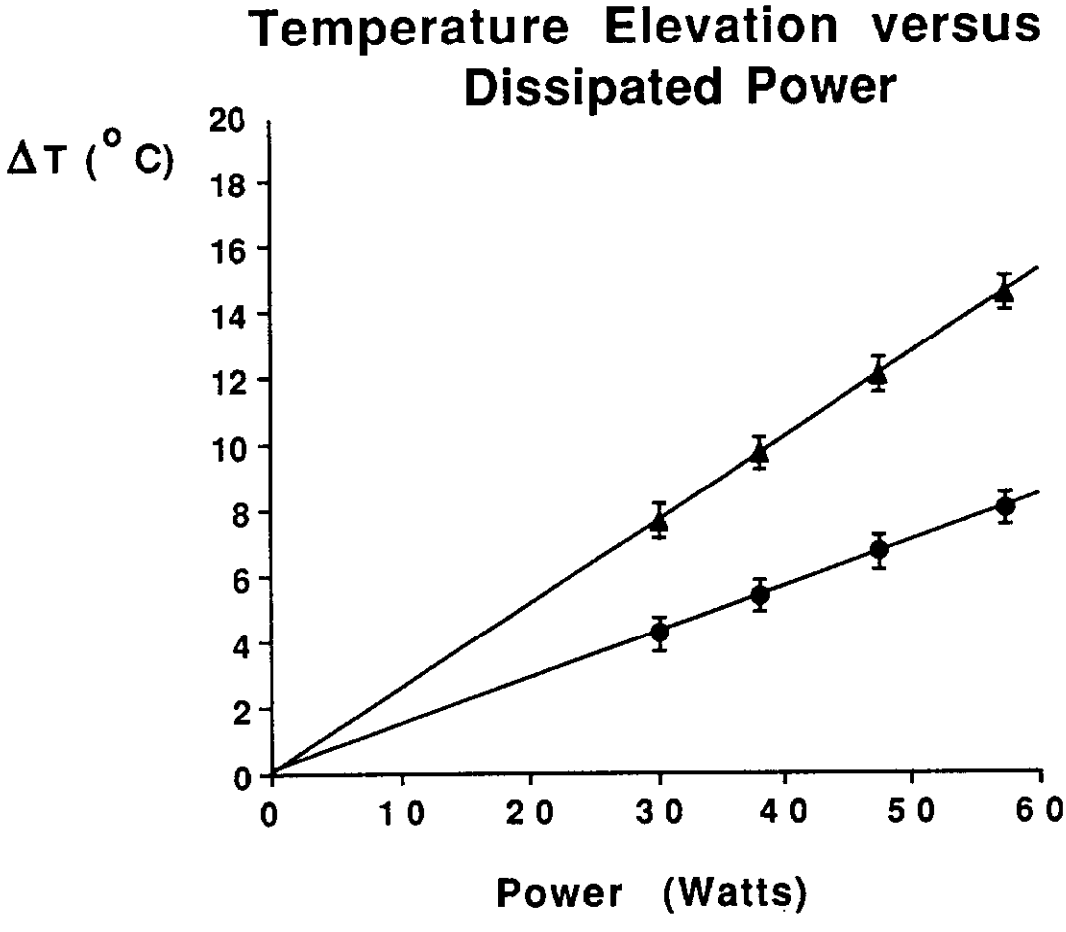
Temperature Elevation versus
Dissipated Power
ΔT (° C)
20
18
16
14
12
10
8
6
4
2
0
0
10
20
30
40
50
60
Power (Watts)

Figure 11

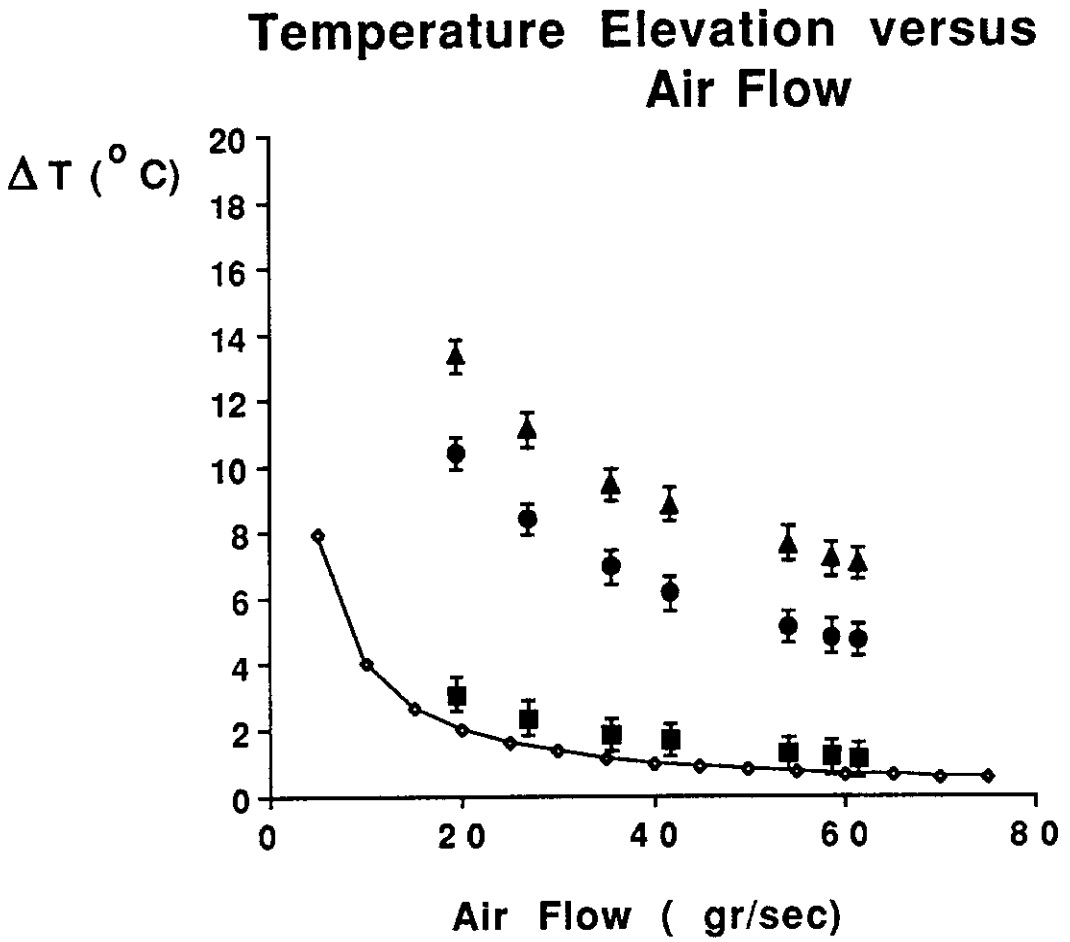
Temperature Elevation versus Air Flow
ΔT (°C)
20
18
16
14
12
10
8
6
4
2
0
0
20
40
60
80
Air Flow (gr/sec)

Figure 12

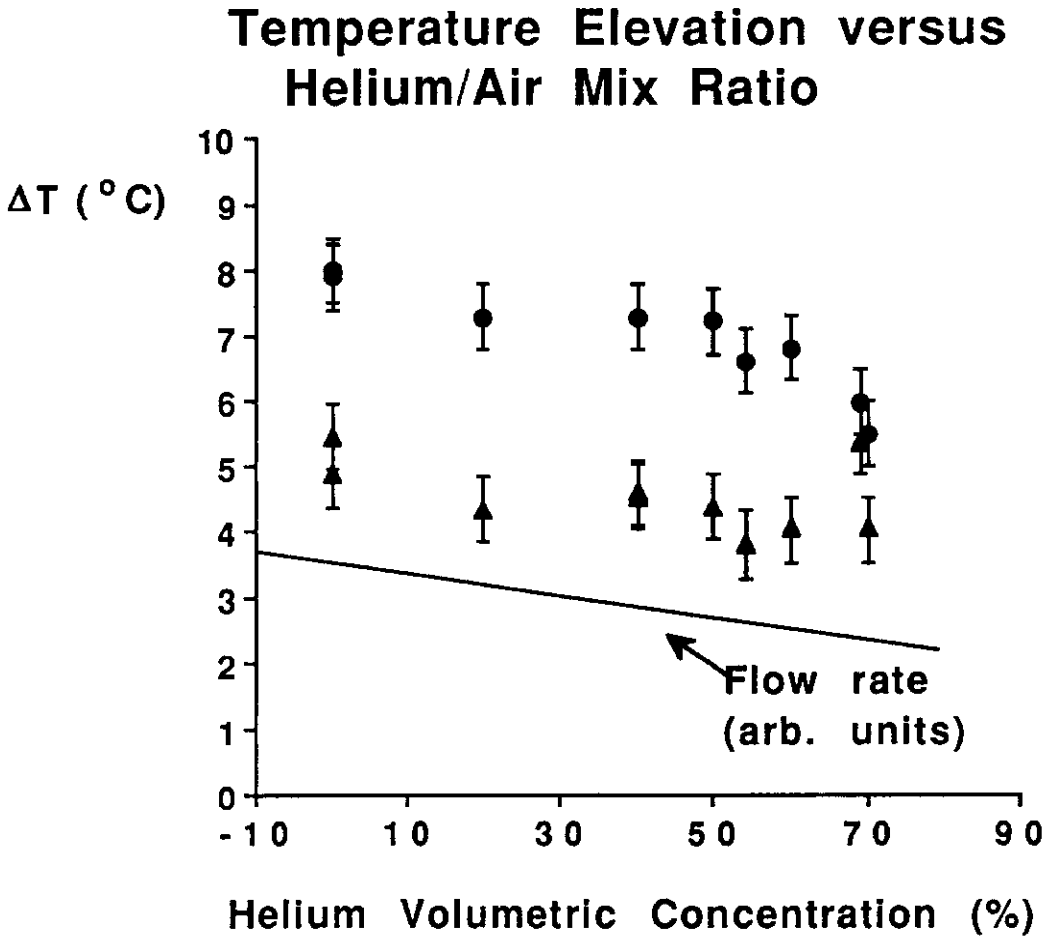
Temperature Elevation versus
Helium/Air Mix Ratio
ΔT (°C)
10
9
8
7
6
5
4
3
2
1
0
-10
10
30
50
70
90
Flow rate
(arb. units)
Helium Volumetric Concentration (%)

Figure 13

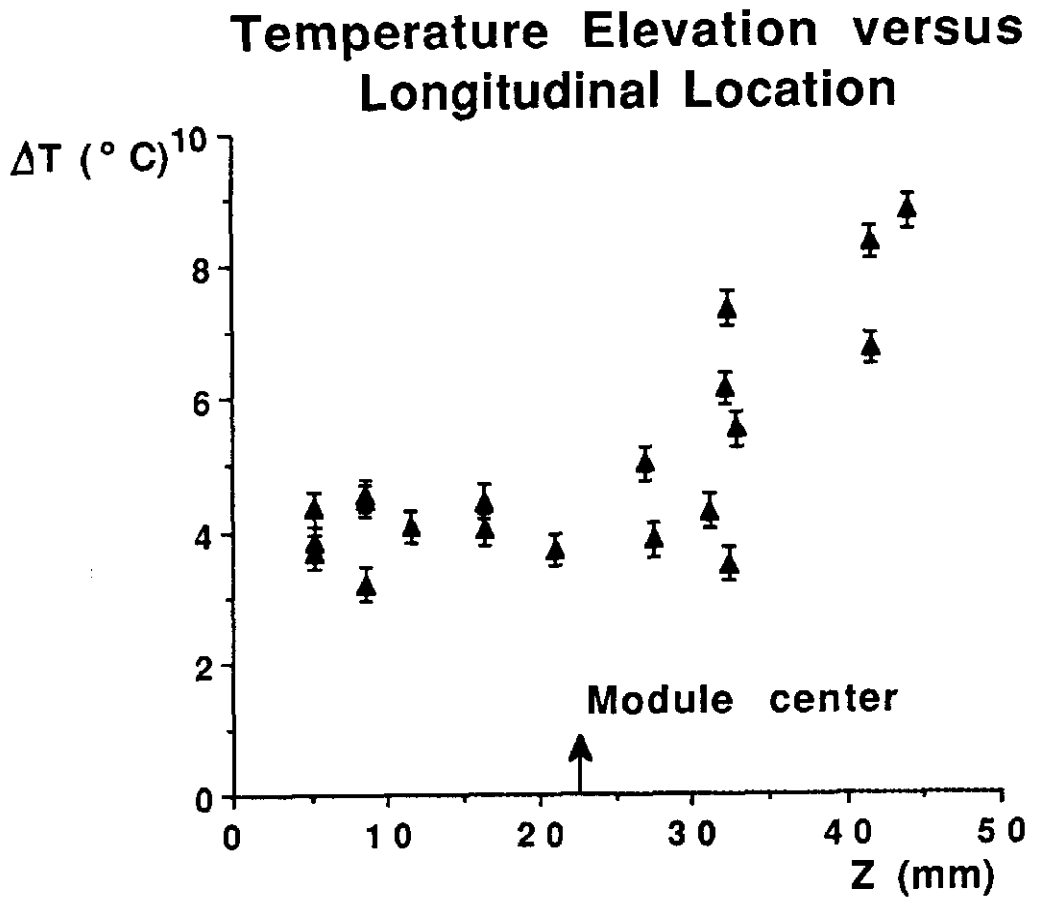
Temperature Elevation versus
Longitudinal Location
ΔT (° C)
10
8
6
4
2
0
Module center
0
10
20
30
40
50
Z (mm)

Figure 14

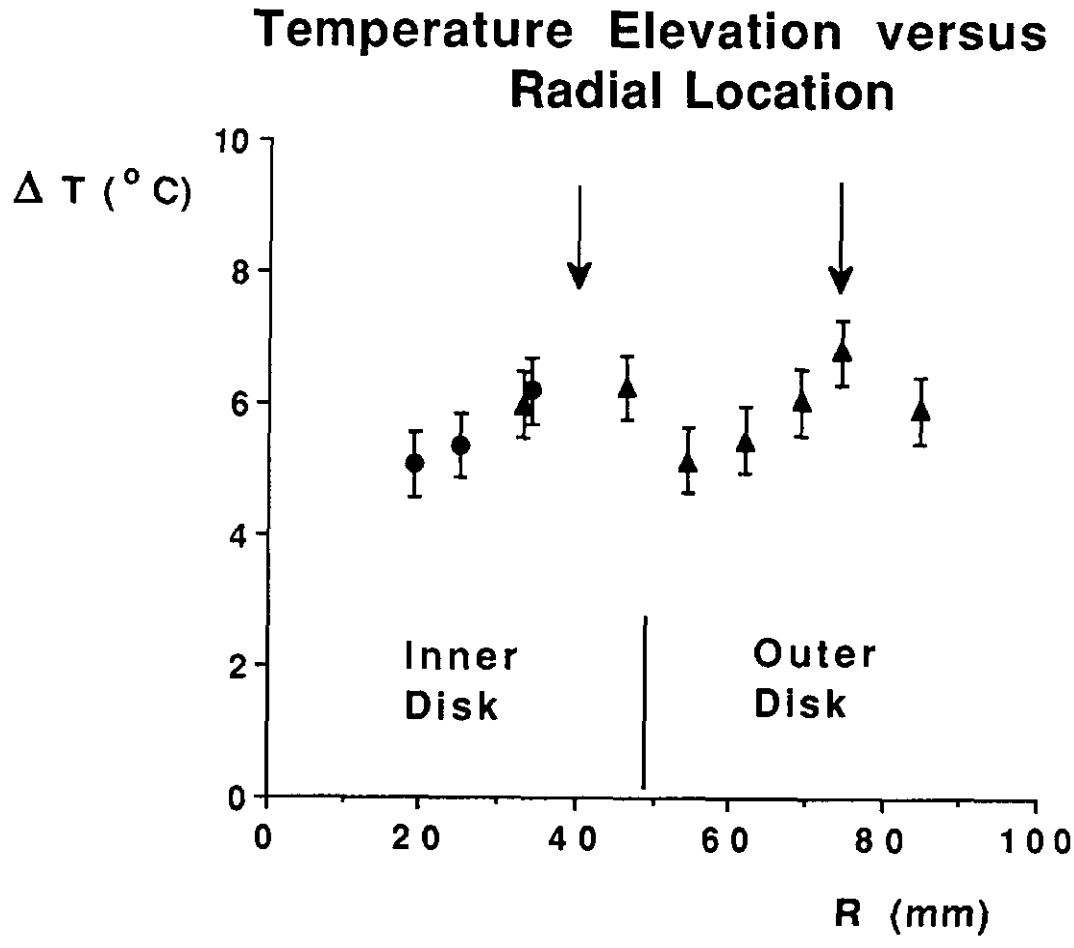
Temperature Elevation versus
Radial Location
Δ T (° C)
10
8
6
4
2
0
Inner
Disk
Outer
Disk
0
20
40
60
80
100
R (mm)

Figure 15